Fabrication and Control of a 6-DOF Magnetic Levitation Stage with Nanopositioning Capability

Won-jong Kim, *Senior Member, IEEE* and Shobhit Verma

Abstract—**This paper presents a compact 6-DOF (degree of freedom) maglev stage that levitates a platen of 0.212 kg and has nanopositioning capability over the linear travel range of 300 μm. A controller was designed and implemented to stabilize the platen. The decoupling between the vertical and horizontal actuation forces was considered and taken care into controller. Various kinds of experiments were carried out to test the capabilities of the system. The experimental results show that the maglev device has a position resolution of better than 2 nm with a maximum velocity of 1 m/s and an acceleration of 30 m/s^2. This positioner can carry an additional payload of 400 g to orient and position the object under nanopositioning precisely. The nominal power consumption is only 15 mW by each horizontal actuator, and 320 mW by each vertical actuator. The potential applications of this maglev device include fabrication of nanoparts and their assembly, vibration isolation for delicate instrumentation, and microscale stereolithography.**

I. Introduction

NANOPOSITIONING and nanomanipulation stages have been in high demands in the last decade. The manufacture of nanoscale devices and their manipulation is essential for the development of the next-generation nanotechnology. The miniaturization of existing manufacturing technologies requires a high-precision positioning stage for the manipulation and fabrication of nano-sized objects. The stage must be able to travel in all directions, and position and orient the object at the desired position with minimum error. This requires high accuracy, large travel range, and simultaneous generation of multi-DOF motions and high control bandwidth.

The most widely used nanomanipulation systems are scanning tunneling microscopes (STMs) and atomic force microscopes (AFMs). The STM has become a common interface for many manipulation systems [1–3]. However these devices have shorter travel ranges on the order of 100 μm and can generate motion in the x-y directions with very small travel in the z direction. Most of these nanomanipulation systems are based on the piezoelectric actuation technology [2, 4]. However, there are several technical challenges with piezoelectric actuators. (1) The accuracy is greatly influenced by thermal drift under temperature variation. (2) The hysteresis in the piezoelectric materials reduces the repeatability in positioning. (3) A slow creeping motion after a large voltage step results in a significant positioning error [5]. Besides piezoactuation systems, there are other types of positioners including a high-speed precision stage with 0.69-nm resolution using a non-resonant-type ultrasonic motor [6]. However, the motion of this system is limited in only one axis.

The magnetic levitation (maglev) technology is proved to be a novel solution for nanomanipulation. Advantages of the maglev technology include the following. (1) Due to absence of friction there is no need of lubricant or precision bearings. This reduces the manufacturing cost significantly. (2) The repeatability and resolution of the system is better due to the absence of backlash, stiction, and friction. (3) No additional moving parts for transmission of force lead to high-bandwidth control and higher natural frequency of the system. (4) The light moving-part mass leads to low power consumption. (5) It is compatible with clean-room or vacuum environments without particulate generation, which is highly suited for the nanotechnology and semiconductor manufacturing.

A 6-DOF planar maglev stage with large planar motion capability was built and demonstrated with 5-nm rms positioning noise and 100-Hz control bandwidth by Kim [7–8]. A long range scanning stage is designed by Holmes, et al. for scanned-probe microscopy that is capable of less than 0.6 nm three-sigma of horizontal positioning noise [9]. This stage has a platen with a 12-kg mass floated in oil to enhance the disturbance rejection and to reduce power consumption. Hajjaji and Ouladsine built a nonlinear control model for long-range movement of a maglev system and tested it by real-time control implementation [10]. Shan, et al. applied robust nonlinear control to their multiple-DOF magnetic suspension stage and demonstrated the nanopositioning capability [11]. Jung and Baek designed and demonstrated a 6-DOF magnetically levitated positioner with self-stability for 5-DOF [12]. This positioner uses air core solenoid and permanent magnets.

The maglev stage discussed here has significant advantages over the existing maglev devices as: (1) There

Manuscript received on September 21, 2003. This material is based upon work supported by the National Science Foundation under Grant No. CMS–0116642.

W.-J. Kim is with Mechanical Engineering Department, Texas A&M University, College Station, TX 77843 USA (phone: 979-845-3645; fax: 979-862-3989; e-mail: wjkim@mengr.tamu.edu).

S. Verma is with Mechanical Engineering Department, Texas A&M University, College Station, TX 77843 USA (e-mail: shobhit@tamu.edu).

is only one lightweight moving part which has high natural frequency due to a stiff structure. (2) There are no parts made of iron so there is no heating due to eddy currents. (3) The moving part consists only of magnets, so there are no power-cables connected to it. This eliminates vibration on platen and avoids heat dissipation due to ohmic loss in the current-carrying coils.

Figure 1 is a photograph of the maglev system we developed. This magnetic levitator has the minimum number of actuators necessary and sufficient for 6-DOF motion generation. Its specifications and dynamic performances include 0.212-kg moving-part mass, 2-nm precision in horizontal motion, 300-μm travel range, 1-m/s speed, 3-*g* acceleration, maximum payload mass of 400 g, higher than 90-Hz control bandwidth, and 15-mW power consumption per horizontal actuator in steady state.

II. Mechanical Design of the Setup

Figure 2 shows the schematic view of the mechanical configuration of the maglev system developed. The triangular part in the center is the platen that is levitated with the help of 3 vertical linear actuators. Maintaining the stiffness high, the mass of the platen was reduced by pocket milling, leaving ribs on the edges and center. On the top surface of the platen there is a viscoeleastic passive damping layer covered by a constraint layer to damp the vibration from resonance. There are 3 sets of protrusions on the sides of triangular platen to hold six magnets for 3 horizontal actuators. These magnets are surrounded by 3 horizontal coils to complete the horizontal actuation scheme of x-y translation and rotation about z. On the three corners of the triangle on the bottom side there are three magnets attached with spacers. These magnets are surrounded by three vertical coils that are attached to base plate with coil holders. This set of coil and magnet forms three actuators and generates motion in the vertical direction. The bottom surface of the platen is bring used as the target of the capacitance gap sensors, so it has been ground to a surface roughness of 2.54 μm. Three plane mirrors are fixed on the sides of the platen by a 127 μm thick double-sided tape.

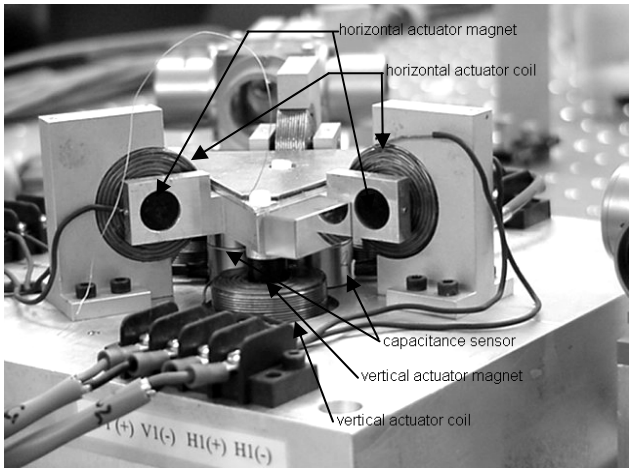

Figure 1: The 6-DOF maglev stage

The 6-DOF motion control is achieved by the application of forces on the platen by 3 vertical actuators and 3 horizontal actuators [13]. Three vertical axes are independently controlled by three vertical actuators and three horizontal actuators control the horizontal motions. Figure 2 shows the description of the directions of the various forces being applied by all the actuators. The experiments for the force corresponding to the position were carried out and optimal position of magnet inside the coil was found [14].

In the magnetic actuators, each cylindrical neodymium-iron-boron (NdFeB) magnet with energy product (BH_{max}) of 0.4 MJ/m^3 (50 MGOe) has the diameter of 11.684 mm and the height of 9.525 mm. The coils for the actuators are made up of single-build AWG#21 (diameter = 0.724 mm) copper magnet wire with 179 turns each. The coils have the inner diameter of 12.2 mm, the outer diameter of 32.5 mm on average, and the height of 9.55 mm. The resistance and the inductance of a coil are 0.552 Ω and 0.5 mH respectively. A professional coil manufacturer, WireWinders, made the coils, and ensured the inner diameter tolerance to be better than 25.4 μm.

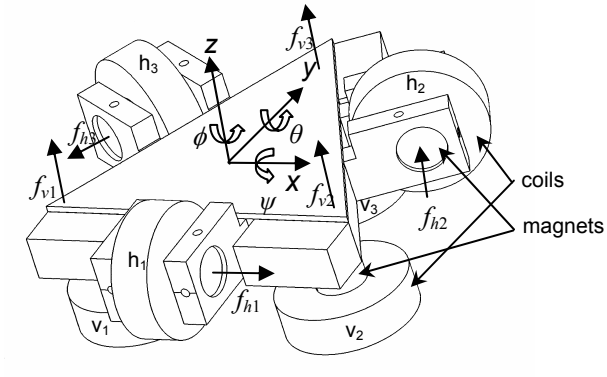

Figure 2: Schematic view of the stage with axes and force definition

III. Dynamic Modeling

A solid model of the mechanical system was developed in Solidworks. The parameters required for system modeling were calculated with the help of the solid model. Due to absence of any kind of stiffness or damping forces this system has been modeled as a pure mass with the dynamic equation as

$$M\frac{d^2X}{dt^2} = F \tag{1}$$

where X and F are displacement and force vectors in the 3 translational axes. Since the mass of the platen is 0.2126 kg, the open loop plant system transfer function for open translation is

$$\frac{X(s)}{F(s)} = \frac{1}{0.2126s^2}. \tag{2}$$

Similarly for rotation

$$\frac{\Theta(s)}{\mathrm{T}(s)} = \frac{1}{Is^2} \tag{3}$$

where, I refers to the moment of inertia around the corresponding axis. T refers to the torque around that axis.

The inertia matrix, taken at the center of mass, obtained using Solidworks (the allocation of axes is shown in Figure 2) is given by:

$$I = \begin{bmatrix} I_{xx} & -I_{xy} & -I_{xz} \\ -I_{yx} & I_{yy} & -I_{yz} \\ -I_{zx} & -I_{zy} & I_{zz} \end{bmatrix} = \begin{bmatrix} 132.88 & -3.14 & 0 \\ -3.14 & 122.28 & 0 \\ 0 & 0 & 235.87 \end{bmatrix} \tag{4}$$

with units in $10^{-6} \times$ kg-m^2. As the products of inertia are less than 3% of the moments of inertia, we neglect them in the present dynamic model.

Translation and rotation in various axes is achieved by combination of forces by 6 linear actuators. The force transformation matrix was found to be

$$\begin{bmatrix} f_z \\ \tau_\theta \\ \tau_\psi \\ f_x \\ f_y \\ \tau_\phi \end{bmatrix} = \begin{bmatrix} 0 & 0 & 0 & 1 & 1 & 1 \\ 0 & 0 & 0 & l_{1x} & -l_{2x} & l_{3x} \\ 0 & 0 & 0 & -l_{1y} & -l_{2y} & l_{3y} \\ -\cos 60^\circ & 1 & -\cos 60^\circ & 0 & 0 & 0 \\ -\cos 30^\circ & 0 & \cos 30^\circ & 0 & 0 & 0 \\ l_{6z} & l_{4z} & l_{5z} & 0 & 0 & 0 \end{bmatrix} \begin{bmatrix} f_{h3} \\ f_{h1} \\ f_{h2} \\ f_{v1} \\ f_{v2} \\ f_{v3} \end{bmatrix} \tag{5}$$

where f_x, f_y and f_z are forces in x, y and z-directions and τ_ψ, τ_θ and τ_ϕ are toques in rotation about ψ, θ and ϕ axes. The definitions of other various forces are shown in Figure 2.

The lengths of physical dimensions are as follows:
l_{1x}: in the x-axis from actuator 4 to y-axis = 2.792 cm;
l_{1y}: in the y-axis from actuator 4 to x-axis = 1.516 cm;
l_{2x}: in the x-axis from actuator 5 to y-axis = 2.708 cm;
l_{2y}: in the y-axis from actuator 5 to x-axis = 1.516 cm;
l_{3x}: in the x-axis from actuator 6 to y-axis = 0.04152 cm;
l_{3y}: in the y-axis from actuator 6 to x-axis = 3.247 cm;
l_{1z}: from actuator 2 to the z-axis = 4.037 cm;
l_{2z}: from actuator 3 to the z-axis = 4.072 cm;
l_{3z}: from actuator 1 to the z-axis = 4.143 cm;

The force generated by the interaction between the permanent magnet and the coil current follows the Lorentz force equation, $\boldsymbol{f} = \int (\boldsymbol{J} \times \boldsymbol{B})\ dV$, where $\boldsymbol{J}$ is the current density flowing through the coil, and $\boldsymbol{B}$ is the magnetic flux density produced by the magnet. The details of this force calculation are given in [14].

The total vertical force with a nominal 1 A current in the three vertical coils is 2.52 N which is sufficient to levitate the platen mass of 0.212 kg against the gravity. The maximum coil current delivered by a power amplifier was set as 2.5 A, which can provide additional 1-g (10 m/s^2) acceleration in the vertical direction and a 3.5-g acceleration in the horizontal direction.

IV. Control System Design

The maglev system was designed so that the 3 vertical DOFs controlled by vertical actuators (z-translation and, ψ- and θ-rotation) are decoupled from the 3 horizontal DOFs (x-and y-translation, and ϕ-rotation). Based on the dynamic model obtained, a continuous time lead-lag controller for each of the 6 axes has been designed using the MATLAB root-locus tool. The controller was designed with the damping ratio ζ as 0.7 and phase margin as 50° at cross over frequency of 50 Hz. To eliminate the steady state error a free pole was allocated at the origin.

$$G_z(s) = \frac{8.7315 \times 10^4 (s+135)(s+11)}{s(s+1385)} \tag{6}$$

The discrete-time model of the controller was found with sampling rate of 5 kHz by ZOH method

$$G_z(z) = \frac{8.7315 \times 10^4 (z-0.9767)(z-0.9978)}{(z-1)(z-0.758)} \tag{7}$$

The controller for the three rotation have same pole-zero location but the gain are different as 96.872 N, 54.575 N, and 50.221 N for ϕ, ψ and θ respectively.

Due to the unmodeled dynamics in the system there are some couplings between vertical and horizontal modes. This effect can be observed clearly in figure 4(a)–(d). To compensate this modeling error, a feedforward decoupling compensation methodology was applied. The compensation torque equal to the output actuation force f_x multiplied by the 3.3-mm moment arm was subtracted to cancel the perturbation in the θ-axis from the x-axis. A similar error torque correction cancels the perturbation in the ψ-axis from the x-axis. The experimental results after the application of this technique are shown in figure 4(e)–(h) that clearly shows a significant improvement in transitional behavior of the system.

V. Experimental Results

Figure 3 shows small step responses and position noises in all six axes. As seen in the figure, the translational position resolution is better than 2 nm in x and y, and 25 nm in z. The lower z-axis resolution stemmed from the larger capacitance sensor and A/D electronics noises. For rotational motions, the angular position resolution is about 2 μrad for ψ and θ, and 200 nrad for ϕ. Figure 4 provides a 20-μm step response in x with the decoupling compensation developed. Because of the abrupt change in acceleration, small-perturbed motions can still be seen in the other 5 axes. However, these perturbations die out quickly due to the controller actions in the other axes. Additional reference trajectories were used to demonstrate the nanoscale motion-control capability of the maglev stage. Figure 5 presents the test results of a square-wave motion with amplitude of 20 nm and a sinusoidal motion with amplitude of 50 nm. The periods of the reference commands were 800 ms and 1 s, respectively. The maglev

stage is capable of following fine commanded motion trajectories and maintaining the same noise level.

VI. Conclusions

Magnetic levitation is a very promising technology for the development of nanoscale positioning stages and other applications. The next-generation nanotechnology needs multi-axis motion generating devices with nano-level resolution like the one we have developed.

In this paper we presented a novel deign of a 6-DOF maglev stage with large travel range and resolution of 2 nm. This device shows better dynamic performance than other existing devices in numerous aspects with less weight and lower power consumption without iron parts or electrical connection to the moving part. The design of the stage with 6 single-axis actuators in a triangular configuration makes this device very compact. The dynamic analysis of the motion includes response of unit actuators along with their mutual coupling due to mechanical transmission.

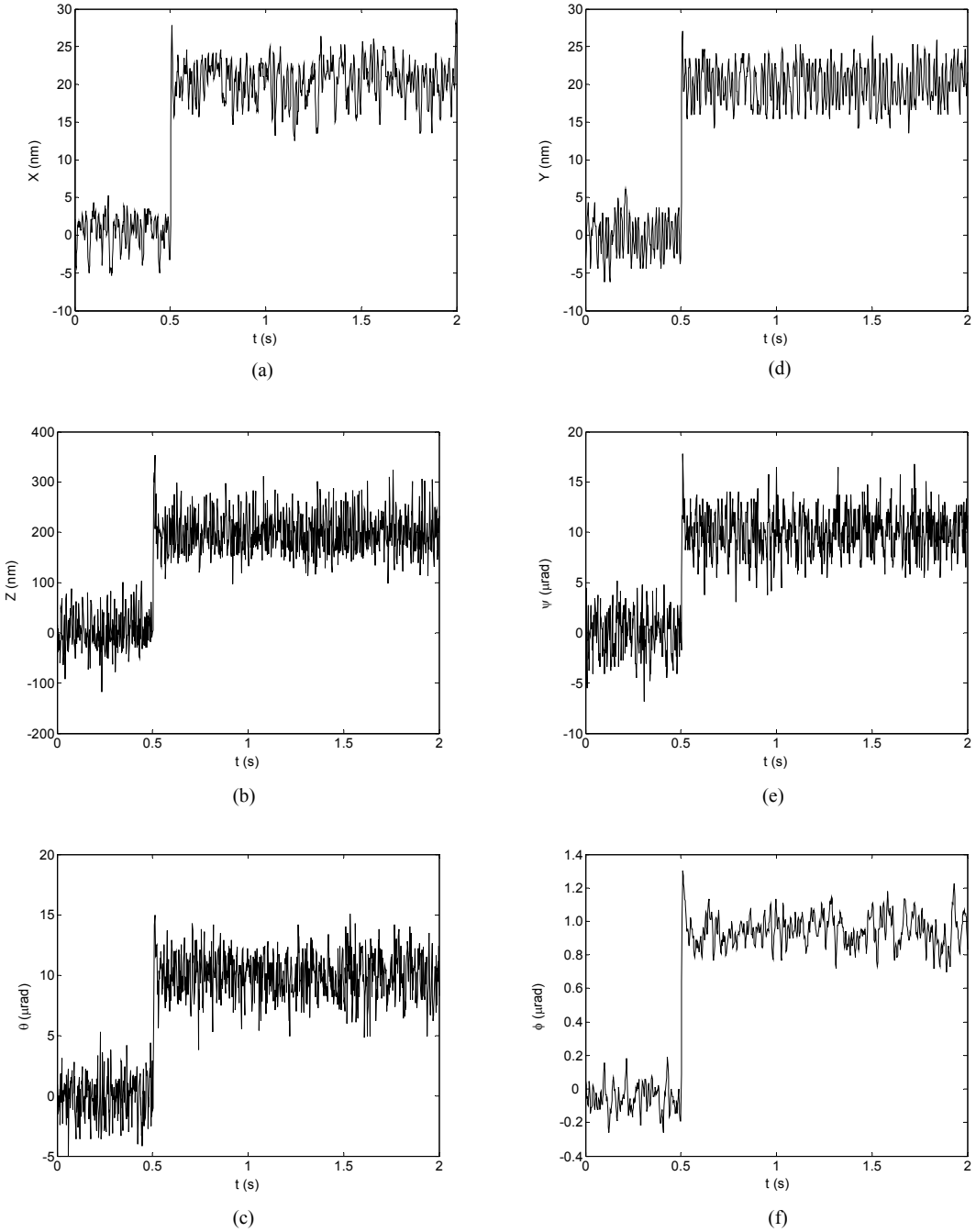

Figure. 3: Various step responses in all six axes with step sizes (a) 20 nm in x, (b) 0.2 μm in z, (c) 10 μrad in θ, (d) 20 nm in y, (e) 10 μrad in ψ, and (f) 1 μrad in ϕ.

The dynamic performance of the maglev system was shown through the step responses in all the 6 axes by a lead-lag controller. This device is capable of positional accuracy of 2 nm, maximum achievable velocity approximately 1 m/s and acceleration of 30 m/s^2 (3 *g*) in horizontal directions and 10 m/s^2 (1 *g*) in vertical direction. The nominal power consumed by vertical actuator is 320 mW and by horizontal actuator is 15 mW.

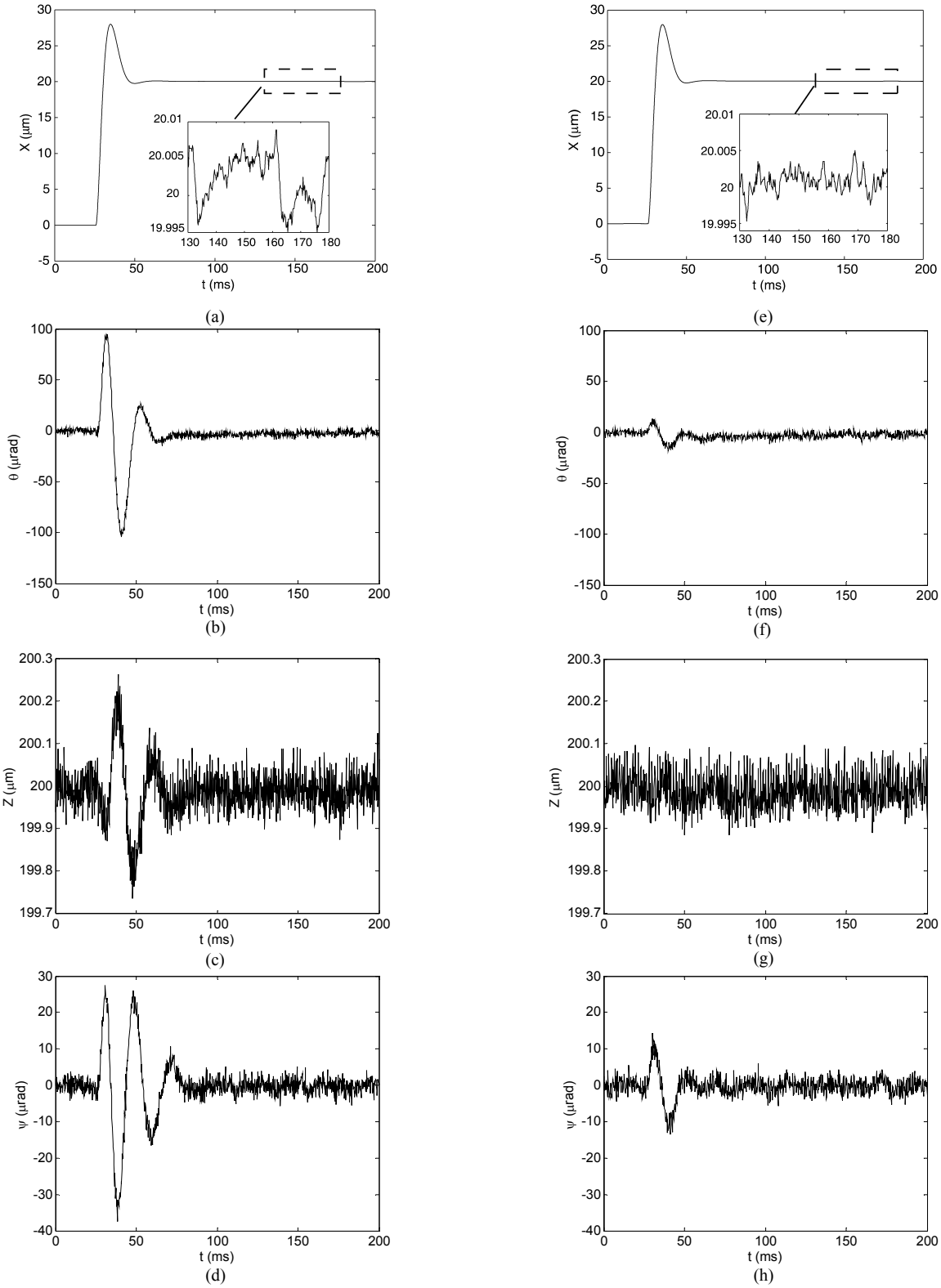

Figure 4: 20-μm step responses in x (a)–(d) without, and (e)–(h) with the decoupling compensation.

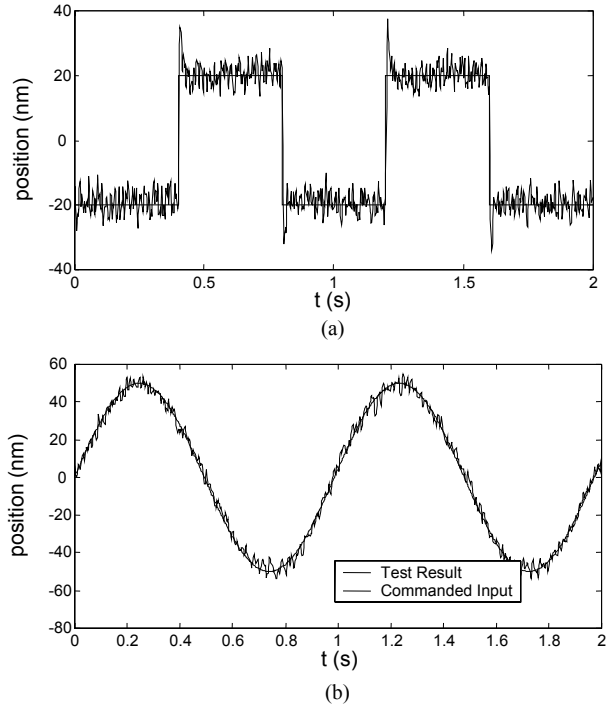

Fig. 5: (a) 20-nm-amplitude square-wave motion in x. (b) 50-nm-amplitude sinusoidal motion in x. The dashed lines represent the commanded input to generate the motion.

This 3-D fine motion generation capability can be used in many applications such as rapid prototyping, precision machining, and precise positioning for microscopic observation of microstructures. The other potential applications include telescopic microsurgery, assembly and packaging of micro-sized parts, and vibration-free delicate instrumentation.

VII. ACKNOWLEDGMENTS

This material is based upon work supported by the National Science Foundation under Grant No. CMS-0116642. We thank Jie Gu for his contributions in the mechanical design and software development.

REFERENCES

[1]. C. Bauer, A. Bugacov, B. E. Koel, A. Madhukar, N. Montoya, T. R. Ramachandran, A. A. G. Requicha, R. Resch, and P. Will, "Nanoparticle Manipulation by Mechanical Pushing: Underlying Phenomena and Real-Time Monitoring," *Nanotechnology*, vol. 9, pp. 360–364, 1999.

[2]. R. M. Taylor, II, *The Nanomanipulator: A Virtual-Reality Interface to a Scanning Tunneling Microscope*, Ph.D. Dissertation, Department of Computer Science, University of North Carolina at Chapel Hill, May 1994.

[3]. M. F. Yu, M. J. Dyer, H. W. Rohrs, X. K. Lu, K. D. Ausman, J. V. Her, and R. S. Ruoff, "Three-Dimensional Manipulation of Carbon Nanotubes under a Scanning Electron Microscope," *Nanotechnology,* vol. 10, pp. 244–252, 1999.

[4]. M. F. Yu, M. J. Dyer, H. W. Rohrs, X. K. Lu, K. D. Ausman, J. V. Her, and R. S. Ruoff, "Three-Dimensional Manipulation of Carbon Nanotubes under a Scanning Electron Microscope," *Nanotechnology*, vol. 10, no. 3, pp. 244–252 1999.

[5]. A. A. G. Requicha, S. Meltzer, A. F. P. Terán, J. H. Makaliwe, H. Sikén, S. Hsieh, D. Lewis, B. E. Koel, and M. E. Thompson, "Manipulation of Nanoscale Components with the AFM: Principles and Applications," *Proc. IEEE-NANO 2001*, pp. 81–86, 2001.

[6]. Y. Egshira, K. Kosaka, S. Takada, T. Iwabuchi, T. Baba, S. Moriyama, T. Harada, K. Nagamoto, A. Nakada, H. Kubota, and T. Ohmi, "0.69 nm Resolution Ultrasonic Motor for Large Stroke Precision Stage," *Proc. IEEE-NANO 2001*, pp. 397–402, 2001.

[7]. W.-J. Kim, *High-Precision Planar Magnetic Levitation,* Ph.D. Dissertation, Massachusetts Institute of Technology, Cambridge, MA, 1997.

[8]. W.-J Kim. and D. L. Trumper, "High-Precision Magnetic Levitation Stage for Photolithography," *Precision Engineering*, vol. 22, pp. 66–77, 1998.

[9]. M. Holmes, R. Hocken, and D. L. Trumper, "The Long-range Scanning Stage: a Novel Platform for Scanned-Probe Microscopy," *Precision Engineering,* vol. 24, pp. 191–209, 2000.

[10]. A. E. Hajjaji and M. Ouladsine, "Modeling and Nonlinear Control of Magnetic Levitation Systems," *IEEE Transactions on Industrial Electronics*, vol. 48, pp. 831–838, 2001.

[11]. X. Shan, S.-K. Kuo, J. Zhang, and C.-H. Menq, "Ultra Precision Motion Control of A Multiple Degrees of Freedom Magnetic Suspension Stage," *IEEE/ASME Transactions on Mechatronics*, vol. 7, pp. 67–78, 2002.

[12]. K. S. Jung and Y. S. Baek, "Development of Novel Maglev Positioner with Self-stabilizing Property," *Mechatronics,* vol. 12**,** pp. 771–790, 2000.

[13]. W.-J. Kim, J. Gu, and H. Maheshwari, "Six-DOF Mechatronic Nanopositioning Device," *Proc. 2nd IFAC Conference on Mechatronics Systems*, pp. 909–914, 2002.

[14]. W.-J. Kim and H. Maheshwari, "High-Precision Control of a Maglev Linear Actuator with Nanopositioning Capability," *Proc. of 2002 American Control Conference*, pp. 4279–4284, 2002.